

# Competition between orthogonally polarized transverse modes in vertical-cavity surface-emitting lasers and its influence on intensity noise

F. Prati,<sup>1,4</sup> G. Giacomelli,<sup>2,5</sup> and F. Marin<sup>3,5</sup>

<sup>1</sup>*Università degli Studi dell'Insubria, Dipartimento di Scienze Chimiche, Fisiche e Matematiche, via Lucini 3, I-22100 Como, Italy*

<sup>2</sup>*Istituto Nazionale di Ottica, Largo E. Fermi 6, I-50125 Firenze, Italy*

<sup>3</sup>*Dipartimento di Fisica, Università di Firenze and LENS, Largo E. Fermi 2, I-50125 Firenze, Italy*

<sup>4</sup>*Istituto Nazionale per la Fisica della Materia, Unità di Ricerca di Milano, I-20133 Milano, Italy*

<sup>5</sup>*Istituto Nazionale per la Fisica della Materia, Unità di Ricerca di Firenze, I-50125 Firenze, Italy*

(Received 6 October 1999; published 14 August 2000)

The influence of transverse modes on the intensity fluctuations of the two orthogonally polarized field components of the electric field in a vertical-cavity surface-emitting laser is analyzed both experimentally and theoretically. It is shown that a very high degree of anticorrelation can be obtained in the presence of bistability between two orthogonally polarized first-order modes.

PACS number(s): 42.55.Sa, 42.65.Pc, 42.50.-p

## I. INTRODUCTION

Vertical-cavity surface-emitting Lasers (VCSELs) are characterized by complicated behaviors involving both transverse modes and the polarization state of the emitted light. Because of their geometry, VCSELs are able to support Gauss-Hermite-like modes and, even at moderate pump levels, they exhibit a multitransverse mode behavior [1–3]. The fact that in these lasers the polarization state of light is less controlled than in conventional edge emitting lasers adds a degree of freedom to transverse-mode competition [4,5]. Several experiments show, for instance, that first-order transverse modes lase orthogonally polarized with respect to the fundamental Gaussian mode [6–9]. Therefore at least two orthogonally polarized transverse modes commonly coexist and compete, and this circumstance may have important consequences for the intensity noise spectra.

In [10] it was shown that incomplete cancellation of the fluctuations in the two polarizations may cause excess noise. The cross correlation between the two orthogonally polarized components of the electric field in that experiment was found to be on the order of  $-0.4$  to  $-0.7$ . An increase in intensity noise caused by energy partition between orthogonally polarized modes was also reported in [11]. Conversely, in [12], squeezing in the total intensity was observed and interpreted as the result of nonclassical correlations between two orthogonally polarized transverse modes. It was demonstrated in [13] that squeezing is possible when the two polarization components have the same intensity or when one of the two is much larger than the other one, i.e., in the limit of single-mode operation.

The role of bistability between orthogonally polarized transverse modes was shown by some of us in [14,15]. The statistical analysis of the intensity fluctuations in the two polarizations suggests that the laser operates in a regime of bistability between two states with approximately the same spatial configuration, but different polarization properties. To simplify as much as possible the description, one can assume that only two transverse modes, the fundamental Gaussian mode  $TEM_{00}$  and, say, the first-order mode  $TEM_{01}$ , are rel-

evant for the dynamics. Bistability is between the state where both modes have the same polarization and a state of mixed polarization. In a bistable system, noise can induce transitions from one state to the other. As a consequence, strongly anticorrelated fluctuations in the two polarization components are observed, the total intensity remaining almost constant. The aim of our paper is to provide a theoretical explanation for such behavior.

Noise-induced polarization hopping in a bistable VCSEL has been studied previously in [16], using the model for polarization dynamics introduced by San Miguel *et al.* in [17]. More recently it was demonstrated that polarization switching can be regarded as a Kramers hopping problem [18], and a simple analytical expression for the two-well potential of the bistable system was derived [19]. However, in these papers the electric field is treated in the plane-wave approximation, a limitation that makes impossible a direct comparison with the results of the experiment described in [14,15], where polarization switching affects first-order transverse modes.

The model adopted in this paper is an extension of [17], which includes different transverse modes similar to those used in [20,21] to numerically study the dynamics of transverse modes in index- and gain-guided VCSELs. We show that with a choice of parameters as close as possible to the experimental ones, the model indeed predicts the existence of a bistable domain. The numerical integration of the dynamical equations, supplemented by noise terms that simulate the effects of spontaneous emission, confirms the existence of a strong anticorrelation in the fluctuations of the two orthogonal polarizations.

The experimental results are summarized in Sec. II. In Sec. III we introduce the model and present the results of the linear stability analysis and a deterministic simulation that demonstrates that a bistable domain exists. The results of the numerical simulations with noise are presented in Sec. IV and compared to the experimental measurements in Sec. V, which also contains some critical remarks.

## II. EXPERIMENTAL RESULTS

The experimental investigations discussed here are described in detail in Refs. [14,15,22]. The lasers have been

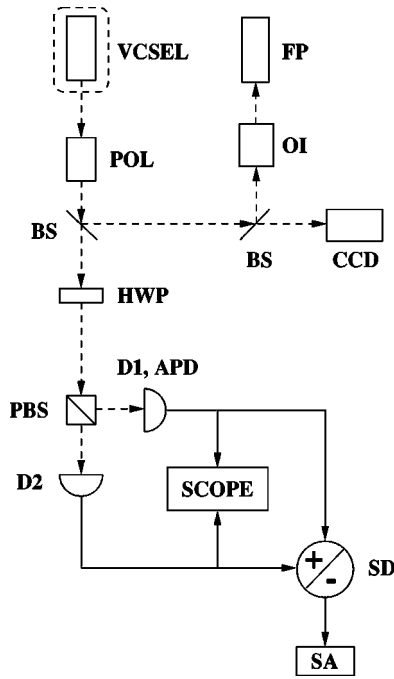


FIG. 1. Experimental setup. POL, polarizer; BS, beamsplitter; OI, optical isolator; FP, Fabry-Perot analyzer; CCD, video camera; HWP, half-wave plate; PBS, polarizing beamsplitter; D1, D2, PIN photodiode with amplifier; APD, avalanche photodiode; SD, sum and difference device; SA, spectrum analyzer.

provided by Centre Suisse d'Electronique et de Microtechnique (Zürich) [23]. The device is an air-post quantum well VCSEL, fabricated by selective lateral etching, with distributed Bragg reflectors. The output window has a diameter of 8  $\mu\text{m}$ . Two perpendicular linear polarizations are defined, parallel and perpendicular to the  $\langle 110 \rangle$  crystal direction [9]. The threshold current is about 5 mA and the differential efficiency is 0.1 W/A near threshold.

The experimental setup is schematically illustrated in Fig. 1. A complete characterization of the laser behavior first requires the determination of spatial structure, polarization, and optical frequency for each of the lasing modes. To this purpose, the different modes are frequency separated by means of a monochromator (instrumental linewidth of 0.06 nm) and two confocal Fabry-Perot spectrum analyzers (with a free spectral range of 2.5 and 3 GHz, respectively). The assignment of the different modes in the transmitted signal of the spectrometers is done using polarizers and moving slits.

Afterwards, the dynamics is investigated by analyzing the fluctuations of the different modes. Two different detection techniques are employed. The laser intensity is observed by means of an avalanche photodetector, whose large bandwidth (about 2 GHz) allows fast details to be uncovered. A couple of balanced PIN detectors allows the measurement of strongly correlated fluctuations and an accurate calibration of the shot-noise level. They exhibit a high quantum efficiency and a precise gain factor, at the expense of a narrower bandwidth (about 20 MHz).

While a detailed description of the experimental findings is reported in the references cited above, we summarize here

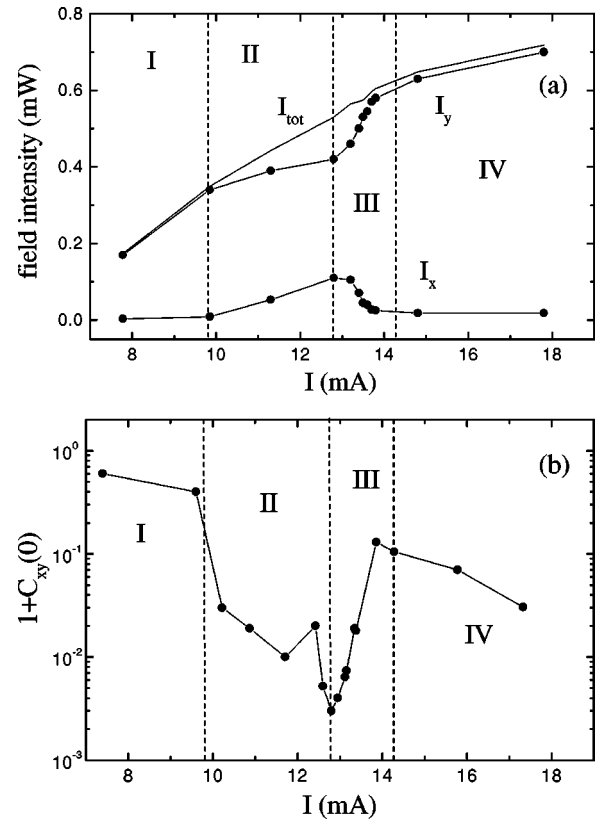


FIG. 2. Experiment. (a) Laser intensity in the principal and in the secondary polarization and (b) deviations from “perfect” anticorrelation [i.e.,  $C_{xy}(0) = -1$ ] between the intensity signals in the two polarizations vs pump current. Regions I–IV are defined by the vertical lines at the currents  $I = 9.8$  mA, 12.8 mA, and 14.3 mA.

the most relevant features that must be considered for the theoretical analysis:

(i) Just above threshold, the laser is well polarized in a single  $\text{TEM}_{00}$  mode belonging to the polarization component which oscillates at the larger frequency. In agreement with the notations of the theoretical model (see Sec. III) we will refer to this polarization axis as “y.”

(ii) Increasing the pump current, the first-order modes appear. In particular, the rise of mode  $\text{TEM}_{01-x}$  (in the orthogonal polarization) leads to anticorrelated polarization fluctuations, with Gaussian statistics.

(iii) Further increasing the pump, mode  $\text{TEM}_{01-x}$  shows large intensity fluctuations and then disappears; in this regime the statistics of the polarization fluctuations are non-Gaussian, displaying fast jumps between two well defined levels. Observing the histograms of the polarized intensity, we deduced that the system is bistable in that region.

These experimental findings are displayed in Figs. 2 and 3. Figure 2(a) shows the average intensities of the two polarization components as functions of the pump current. In regions I and IV the intensity of the secondary polarization is almost equal to zero while in regions II and III mode  $\text{TEM}_{01-x}$  is active. The boundary between the two regions is defined by the value of the pump current at which the average intensity of the secondary polarization is maximum.

In Fig. 2(b) we plot as a function of the pump current the quantity  $1 + C_{xy}(0)$ ,  $C_{xy}(\tau)$  being the correlation between

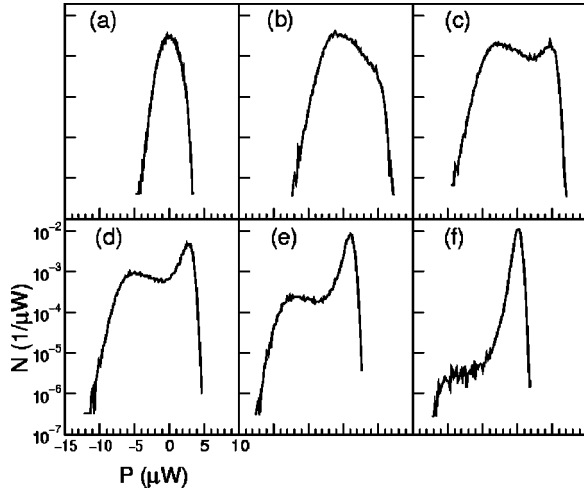


FIG. 3. Experiment. Histograms of the intensity signal for the principal polarization at different values of the pump current:  $I = 10.9$  mA (a),  $12.4$  mA (b),  $12.8$  mA (c),  $13.0$  mA (d),  $13.1$  mA (e), and  $13.5$  mA (f). The histograms are normalized in such a way that the area is the relative noise.

the intensity signals of the two polarizations, which will be defined explicitly in Sec. III. The logarithmic scale allows one to appreciate the high level of anticorrelation in the transition region from II to III. The maximum level of anticorrelation is  $C_{xy}(0) \approx -0.997$ .

Finally, Fig. 3 shows the intensity histograms of the principal polarization for six values of the pump current around the point of maximum anticorrelation. The two maxima of the histograms, visible for some current values, can be associated with two metastable states. Interpreting the histograms as quasipotentials [24], we can establish a relation between the variations of the histogram shape and the crossing of the bistable region, increasing the pump current [15]. In fact, we cannot observe directly a bistability because of the intrinsic noise of the system, which forces the jumps between the two states. However, as shown in Sec. III, the model confirms such a deduction.

In order to realistically modelize the laser behavior, we have performed a series of preliminary measurements, of the frequency splittings among the different laser modes. From these measurements, important parameters of the laser, such as birefringence (see Sec. III), can be evaluated.

We found that the frequency of the  $TEM_{00-y}$  mode is about 80–100 GHz lower than that of the first-order modes (the splitting increases with the pump current at a rate of about 2 GHz/mA). The  $TEM_{10-y}$  and the  $TEM_{01-x}$  modes are at the same frequency, while the  $TEM_{01-y}$  mode is split at a higher frequency (the splitting is 8 GHz, increasing at a rate of 1 GHz/mA). The cavity linewidth  $\kappa$  can be deduced from the structure of the laser cavity and corresponds to about  $1200 \text{ ns}^{-1}$ .

### III. THEORETICAL ANALYSIS AND DETERMINISTIC BEHAVIOR

Our theoretical analysis is based on the model introduced by San Miguel, Feng, and Moloney in [17], which will be

named SFM in the following. This denomination has a double meaning: it refers to the initials of the authors of that paper, but it could be also intended as the acronym for the spin-flip model, indicating that spin-flip processes between the two carrier subpopulations  $N_+$  and  $N_-$  with opposite values of the total angular momentum are one of the main ingredients of the model [25]. In the Cartesian basis  $(E_x, E_y)$ , the equations of SFM read

$$\dot{E}_x = -(\kappa + \eta + i\sigma)E_x + \kappa(1 + i\alpha)(NE_x + inE_y), \quad (1)$$

$$\dot{E}_y = -(\kappa - \eta - i\sigma)E_y + \kappa(1 + i\alpha)(NE_y - inE_x), \quad (2)$$

$$\dot{N} = -N(1 + |E_x|^2 + |E_y|^2) - in(E_yE_x^* - E_xE_y^*) + \mu, \quad (3)$$

$$\dot{n} = -n(\Gamma + |E_x|^2 + |E_y|^2) - in(E_yE_x^* - E_xE_y^*). \quad (4)$$

Here time has been scaled to the recombination time  $\gamma^{-1}$ ,  $\kappa$  is the cavity linewidth,  $\Gamma$  is the spin-flip rate,  $\eta$  and  $\sigma$  are amplitude and phase anisotropy parameters related to dichroism and birefringence, respectively. All these parameters are scaled to  $\gamma$ . In particular, the birefringence parameter  $\sigma$  represents one half of the scaled frequency difference of the two linearly polarized components  $E_x$  and  $E_y$  of the electric field

$$\sigma = \frac{\omega_y - \omega_x}{2\gamma}. \quad (5)$$

Considering positive values of  $\sigma$ , as we do in this paper, amounts to defining the  $y$ -polarized component of the electric field as the one oscillating at the larger frequency. The carrier populations  $N$  and  $n$  are defined as  $N = (N_+ + N_-)/2$  and  $n = (N_- - N_+)/2$ . Finally,  $\alpha$  is the linewidth enhancement factor and  $\mu$  is the pump parameter, proportional to the intensity of the injected current.

As shown in [26], the  $x$ - and  $y$ -polarized solutions have different stability domains and this provides a theoretical explanation for the polarization switchings that are commonly observed in vertical cavity semiconductor lasers. Although the equations are derived in the plane-wave approximation, they can be easily adapted for fields with a Gaussian profile [27].

In this paper we extend the analysis to the situation where the first-order transverse modes are also active. In the experiment, the two modes  $TEM_{01-x}$  and  $y$  polarized were detected, but only the mode  $TEM_{10-y}$  polarized was detected [22]. This asymmetric behavior cannot be explained in a simple way by the model, in the sense that if the four first-order modes are included with the same losses, all of them participate in the dynamics. Therefore since we are interested mainly in the dynamics caused by the polarization switchings of mode  $TEM_{01}$ , we decided to consider only those modes and the fundamental ones. Accordingly, each component of the electric field is written as

$$E_x(x, y, t) = \sum_{i=1}^2 A_i(x, y) f_{i,x}(t), \quad (6)$$

$$E_y(x, y, t) = \sum_{i=1}^2 A_i(x, y) f_{i,y}(t), \quad (7)$$

where

$$A_1(x, y) = \sqrt{\frac{2}{\pi}} e^{-(x^2+y^2)}, \quad (8)$$

$$A_2(x, y) = \sqrt{\frac{2}{\pi}} 2ye^{-(x^2+y^2)} \quad (9)$$

are the modal functions that describe, respectively, the fundamental Gaussian mode  $TEM_{00}$  and the first-order mode  $TEM_{01}$ . Here the transverse coordinates  $x$  and  $y$  are scaled to the beam waist of the fundamental Gaussian mode.

Gauss-Hermite modes are not in general exact eigenmodes for a vertical cavity laser, but we are confident that they represent a good approximation of the real modes. These modes are exact solutions of the wave equation in the presence of a parabolic profile of the refractive index. Under these conditions, which can be attributed to thermal lensing, one can derive the dynamical equations for mode amplitudes  $f_{j,x}$ ,  $f_{j,y}$  [28]:

$$\begin{aligned} \dot{f}_{j,x} = & -(\kappa + \eta - ia\delta_{j,2} + i\sigma)f_{j,x} + \kappa(1 + i\alpha) \\ & \times \int_{-\infty}^{\infty} dx \int_{-\infty}^{\infty} dy A_j(NE_x + inE_y), \end{aligned} \quad (10)$$

$$\begin{aligned} \dot{f}_{j,y} = & -(\kappa - \eta - ia\delta_{j,2} - i\sigma)f_{j,y} + \kappa(1 + i\alpha) \\ & \times \int_{-\infty}^{\infty} dx \int_{-\infty}^{\infty} dy A_j(NE_y - inE_x). \end{aligned} \quad (11)$$

The parameter  $a$  is the scaled frequency spacing between modes  $TEM_{01}$  and  $TEM_{00}$ :

$$a = \frac{\omega_{01} - \omega_{00}}{\gamma}. \quad (12)$$

The equations for  $N$  and  $n$  coincide with Eqs. (3) and (4), even in the multitransverse-mode model. It must be taken into account, however, that now  $N$  and  $n$  are functions not only of time but also of the transverse coordinates  $x, y$ . A dependence on  $x$  and  $y$  may also be assumed for the pump parameter  $\mu$ , in order to take into account the finite cross section of the active region. To simplify both analytical and numerical calculations we assumed that the injected current has a Gaussian profile, with width  $\psi$ :

$$\mu(x, y) = \mu \exp\left(-2\frac{x^2+y^2}{\psi^2}\right). \quad (13)$$

With this assumption, the fundamental Gaussian mode has the lowest threshold, given by  $\mu_{\text{thr}} = 1 + 1/\psi^2$ .

The smoothening of the transverse profile of the carrier density described by Eq. (13) could be attributed to carrier diffusion. A rigorous description of the effects of carrier dif-

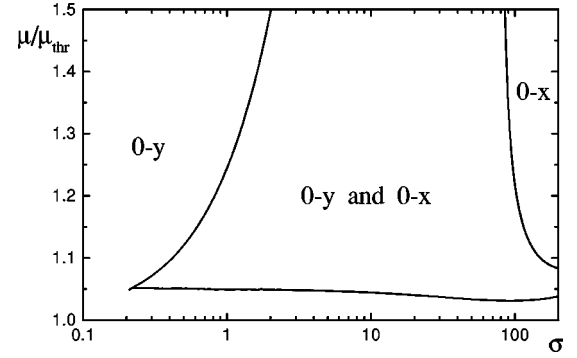


FIG. 4. Stability domains of modes  $TEM_{00}$   $x$  and  $y$  polarized for  $\kappa = 600$ ,  $\Gamma = 300$ ,  $\eta = 0.05$ ,  $\alpha = 2$ , and  $\psi = 3$ .

fusion would greatly complicate the theoretical analysis, because the presence of the Laplacian in the equations for carriers makes it impossible even to determine analytically the stationary states of the laser. However, numerical simulations performed in [29] have shown that, for what concerns the stability of first-order modes, the effects of carrier diffusion are mainly quantitative, in the sense that the stability domains are simply shifted toward higher values of the pump current. An explanation for this is that carrier diffusion partly refills the spatial hole burnt by the lasing mode, making it more stable. If we were interested in a direct comparison between the observed values of the pump current  $I$  at the lasing thresholds of the different modes, and the corresponding values of the pump parameter  $\mu$ , we should take into account carrier diffusion. But this comparison is made problematic by the absence of any precise information about the relationship between  $\mu$  and  $I$ . For these reasons we believe that, for the purposes of this paper, carrier diffusion can be neglected.

The parameters that appear in the model are  $\kappa$ ,  $\Gamma$ ,  $\eta$ ,  $\sigma$ ,  $a$ ,  $\alpha$ , and  $\psi$ . For some of them we have a direct estimation from the experiment. Assuming  $\gamma = 2 \text{ ns}^{-1}$ , the scaled cavity linewidth is  $\kappa = 600$ , the birefringence parameter is  $\sigma \approx 12.5$ , and the frequency spacing is  $a \approx 300$ . The dichroism parameter  $\eta$  is unknown, but it has to be positive in order to reproduce in the numerical simulations the observed preference for the high-frequency ( $E_y$ ) component of the electric field. We assumed  $\eta = 0.05$ . The spin-flip rate  $\Gamma$  has been recently measured in a VCSEL [30] and the value  $\Gamma = 290 \pm 100$  was found. In this paper we set  $\Gamma = 300$ . As for the remaining parameters  $\alpha$  and  $\psi$ , we chose the values  $\alpha = 2$  and  $\psi = 3$ , because they maximize the extension of the bistable domain.

In Fig. 4, the stability domains for the two fundamental modes  $x$  and  $y$  polarized are shown. Due to the positive value of  $\eta$ , the only stable mode close to threshold is always the  $y$ -polarized one. Even when increasing the pump, the bistable domain is reached, the laser keeps emitting on the  $y$ -polarized mode. A switch to the  $x$ -polarized mode is possible only for values of the birefringence parameter  $\sigma$  that are much larger than the experimental one, for which this mode is the only stable solution of the laser. Thus with our choice of parameters, the fundamental mode is always  $y$  polarized, and it never switches to the orthogonal polarization,

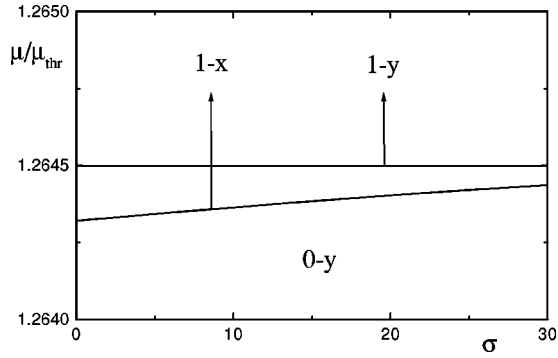


FIG. 5. Instability thresholds of mode  $TEM_{00}$   $y$  polarized with respect to the two first order modes  $TEM_{10}$   $x$  and  $y$  polarized. Same parameters as in Fig. 4 and  $a = 300$ .

in agreement with the experiment.

The instability thresholds of the  $y$ -polarized fundamental mode with respect to the two first-order modes,  $x$  and  $y$  polarized, are shown in Fig. 5. In spite of the fact that the  $y$ -polarized modes are favored by dichroism, the  $y$ -polarized fundamental mode is first destabilized by the  $x$ -polarized first-order mode, at least for moderate birefringence. This result, which agrees with several previous observations [6–9], is also of fundamental importance for the interpretation of our experiment, because it is at the basis of the bistable behavior that can be observed sweeping the pump parameter  $\mu$  adiabatically forward and backward.

The bistable cycle is shown in Fig. 6, where  $\mu/\mu_{thr}$  varied from 1.25 to 1.4 and back in 30  $\mu s$ . In the forward sweep, in agreement with the stability analysis, we observe the growth of mode  $TEM_{01}$   $x$  polarized, starting from about  $\mu = 1.265\mu_{thr}$ . But, since we are in parametric conditions that are favorable for the  $y$ -polarized modes, at about  $\mu = 1.35\mu_{thr}$  mode  $TEM_{01}$   $y$ -polarized also starts growing. The two first-order modes coexist until about  $\mu = 1.38\mu_{thr}$ , where the  $x$ -polarized modes switch off, and the laser emits on the two  $y$ -polarized modes. In the backward sweep, the situation does not change until, at about  $\mu = 1.32\mu_{thr}$ , the first-order mode switches from the  $y$  to the  $x$  polarization. In this way, hysteresis cycle is realized. Bistability is between the state where both modes are  $y$  polarized and a state of mixed polarization.

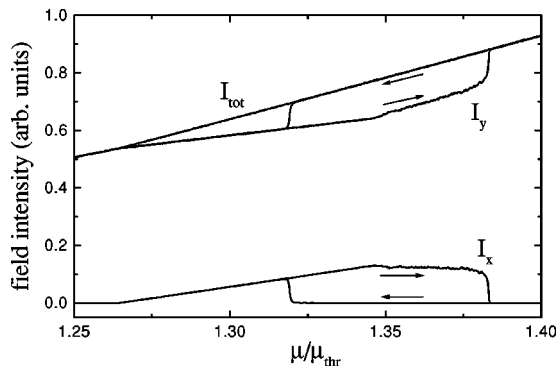


FIG. 6. Bistability domain obtained by an adiabatic sweep, forward and backward, of the pump parameter  $\mu$ . Same parameters as in Fig. 5, with  $\sigma = 12.5$ .

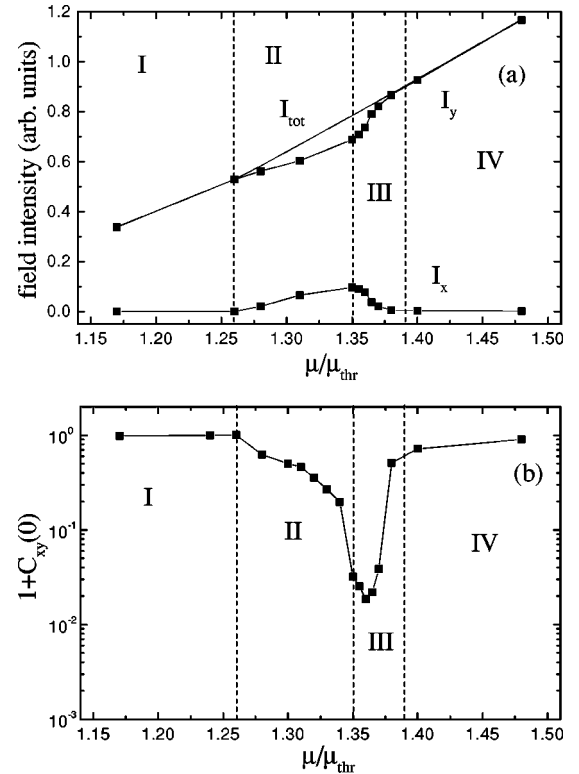


FIG. 7. Same as Fig. 2 for numerical simulations. Regions I–IV are defined by the vertical lines at the pump values  $\mu = 1.26\mu_{thr}$ ,  $\mu = 1.35\mu_{thr}$ , and  $\mu = 1.39\mu_{thr}$ .

#### IV. NUMERICAL SIMULATIONS WITH NOISE

A comparison with the experiment requires the inclusion of noise in the dynamical equations. Sources of Gaussian white noise  $\zeta_{i,j}(t)$  ( $i = x, y, j = 1, 2$ ) were added to the equations for mode amplitudes in order to simulate the effects of spontaneous emission. The complex functions  $\zeta_{i,j}(t)$  have a zero mean value and are  $\delta$  correlated in time [16]:

$$\langle \zeta_{i,j}(t) \rangle = 0, \quad (14)$$

$$\langle \zeta_{i,j}(t) \zeta_{k,l}(t') \rangle = 0, \quad (15)$$

$$\langle \zeta_{i,j}^*(t) \zeta_{k,l}(t') \rangle = \beta \delta_{i,k} \delta_{j,l} \delta(t-t'). \quad (16)$$

The absence of correlation for noise sources of different modes with the same polarization follows from the orthogonality of the modes [31]. We adopted the value  $2 \times 10^{-4}$  for the parameter  $\beta$ , which measures the strength of noise. For each pump value we integrated the dynamical equations for 50  $\mu s$ , recording  $10^5$  data, with a sampling rate of 2 Gsamples/s, identical to that of the experiment. The time step was 0.5 ps.

As a first effect of noise, we observed the disappearance of the hysteresis cycle. In fact, in a pictorial way, one can imagine that the system in the bistable domain is described by a two-well potential. The shape of the potential changes inside the domain. In proximity of the extrema, one well is much more shallow than the other. In these conditions even a small quantity of noise is able to force the system to switch

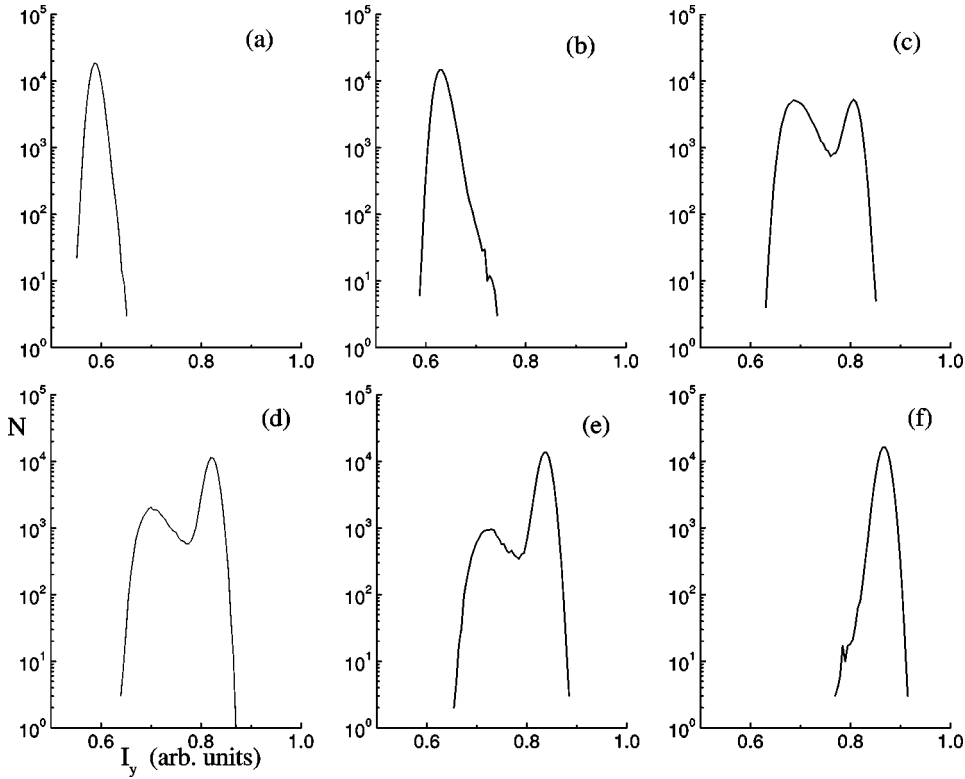


FIG. 8. Same as Fig. 3 for numerical simulations.  $\mu = 1.3\mu_{\text{thr}}$  (a),  $\mu = 1.33\mu_{\text{thr}}$  (b),  $\mu = 1.36\mu_{\text{thr}}$  (c),  $\mu = 1.365\mu_{\text{thr}}$  (d),  $\mu = 1.37\mu_{\text{thr}}$  (e),  $\mu = 1.38\mu_{\text{thr}}$  (f).

to the state corresponding to the deeper well, even if it started in the other state. If noise is not too large, the system will then remain forever in the deeper well. In these conditions bistability cannot be observed, since it stems from the fact that the system can remain in the shallower well. In the central part of the bistable domain the two wells have comparable depth. In this case noise makes the system switch continuously from one state to the other and back, and strong fluctuations appear.

In Fig. 7 we show the results of our numerical simulations in a way that allows a direct comparison to be made with the experimental results shown in Fig. 2. The meaning of regions I to IV is the same in both figures. Regions I and IV are those where the secondary polarization  $I_x$  is negligible; the boundary between regions II and III is represented by the pump value at which the secondary polarization is maximum. In the numerical simulations this maximum is placed at  $\mu = 1.35\mu_{\text{thr}}$ .

The properties of the intensities fluctuations are described by the cross-correlation function defined as

$$C_{xy}(\tau) = \frac{\langle \Delta I_x(t+\tau) \Delta I_y(t) \rangle}{\sqrt{\langle \Delta I_x^2(t) \rangle \langle \Delta I_y^2(t) \rangle}}. \quad (17)$$

The quantity  $1 + C_{xy}(0)$  is 0 for perfect anticorrelation, 1 for no correlation, and 2 for perfect correlation. The behavior of the correlation is very different in the four regions. Unlike in the experiment, the point of maximum anticorrelation does not coincide with the point where the secondary polarization is maximum, but it is placed close to it, at  $\mu = 1.36\mu_{\text{thr}}$ . At this point the correlation is  $C_{xy}(0) \approx -0.982$ .

Figure 8 shows the intensity histograms for the main po-

larization  $I_y$ , obtained for values of the pump close to the point of maximum anticorrelation. The histograms show the transition from the lower to the upper state. They provide an upside down representation of the generalized potential, with the two peaks in the histograms of Figs. 8(c)–8(e) corresponding to the two wells in the potential.

## V. COMPARISON WITH THE EXPERIMENT AND CONCLUSIONS

In this final section we compare the experimental findings with the numerical results derived from the model. The comparison of the average intensities in the two polarizations [Figs. 2(a) and 7(a)] of the cross-correlation function [Figs. 2(b) and 7(b)] and of the histograms of the main polarization around the point of maximum anticorrelation (Figs. 3 and 8) show very good agreement between the experiment and the numerical results based on SFM.

In particular, we remark that excellent agreement is found for the following aspects.

(i) *Preference for a given polarization.* Just above threshold, the laser emits a single mode  $\text{TEM}_{00}$ , well polarized along a plane that is always the same every time the laser is switched on. Even for larger pump currents, mode  $\text{TEM}_{00}$  never switches to the orthogonal polarization. The mode belongs to the polarization component that oscillates at the higher frequency, i.e., the  $y$  component in the theoretical model. This behavior can easily be reproduced in the simulations assuming that the  $y$  component is favored by dichroism. As shown in Fig. 4, if this component is stable at threshold, it remains stable for any value of the pump for the adopted value of the birefringence parameter  $\sigma$ .

(ii) *Bistability*. At a certain pump current, a first-order mode starts oscillating in the secondary polarization. Further increasing the current, this mode switches to the principal polarization. On the basis of the analysis of the intensity histograms, such a switching was interpreted in [15] as the manifestation of a bistable behavior of the laser. Such a bistability is also found in the numerical simulations, as a consequence of the fact that the fundamental Gaussian mode  $y$  polarized is first destabilized by a first-order mode  $x$  polarized.

(iii) *Anticorrelation in the intensity fluctuations*. In both the experiment and the numerical simulations we found that the intensity fluctuations in the two orthogonally polarized components of the electric field can reach very high levels of anticorrelation in the presence of bistability.

There are also some discrepancies between theory and experiment. The most relevant consists in the fact that the correct order of appearance of the first-order modes is not reproduced exactly in the numerical simulations. In the experiment, at the rise of the secondary polarization both modes  $TEM_{01} y$  and  $TEM_{10} y$  are already lasing [22]. Conversely, in the numerical simulations the first mode that grows is mode  $TEM_{01} x$ , and this is a necessary condition for bistability. Moreover, bistability disappears when modes  $TEM_{10}$  are included in the model with the same losses as modes  $TEM_{01}$ .

There are many possible reasons for this different behavior. For instance, it is known that the linear anisotropies of the laser are not constant but vary with the intensity of the pump current. The dependence of birefringence on the pump current was measured, but we did not include it in the theoretical analysis because it has negligible consequences on the stability properties of the different modes. Conversely, such properties could be greatly influenced by even small changes of the parameter  $\eta$ , which describes dichroism, and the sequence of bifurcations could be more complex than the one obtained with  $\eta$  constant. However, in the absence of any precise experimental measurement, we preferred not to add any *ad hoc* hypothesis just to fit the experimental data.

Another possible explanation for the different behavior could be that Gauss-Hermite modes represent only a first approximation of the real modes of a VCSEL. A more precise determination of the field profiles of the different modes could reveal different stability properties.

However, as a general comment, it must be observed that in the numerical simulations mode  $TEM_{01} y$  appears at about the middle of the hysteresis cycle, where the secondary intensity  $I_x$  stops growing (Fig. 6). So, at least in the right part of the bistable domain, the simulations faithfully reproduce the experimental observations, with both of the two orthogonally polarized modes  $TEM_{01}$  above threshold.

These considerations probably help to explain another difference between experiment and simulations, namely, the very different degree of anticorrelation, especially in region II, where the measured correlation is about  $-0.98$ , while in numerical simulations it varies from  $-0.4$  to  $-0.75$ . The point is that in numerical simulations in a large part of region II mode  $TEM_{01} y$  is still below threshold, and hence the dominant fluctuations are those of the two modes  $TEM_{00} x$  and  $TEM_{01} x$ , which, being only partially overlapped, display a small degree of anticorrelation.

The anticorrelation observed in numerical simulations remains smaller than the experimental one even in region III, but there the differences are smaller. For instance, the minimum value of  $C_{xy}(0)$  is  $-0.982$  in the numerical simulations and  $-0.997$  in the experiment. This discrepancy could be related to the fact that in the numerical simulations the ratio  $I_x/I_y$  is always smaller than in the experiment. This means that the relative weight of first-order modes to the fundamental one is smaller; since the total anticorrelation is due essentially to the fluctuations of the first-order modes, this may explain the lower level found in the numerical simulations. It must also be taken also into account that in the numerical simulations the fluctuations of the fields are analyzed inside the cavity, while in the experiment the measurements are obviously performed outside.

Finally, we observe that, while in the model used in this paper and in the Langevin equation with quasipotentials adopted in [15] it is assumed that the dynamics is generated by stochastic fluctuations, the polarization jumps could just as well be produced by a strictly deterministic dynamics. In order to discriminate between noisy and deterministic dynamics we performed a fractal dimension analysis of the experimental data in the transition regime using the Grassberger-Procaccia algorithm [32]. We found no convergence of the method, with a dimension increase with the embedding dimension up to 10. We conclude that either the dynamics is high dimensional, or the possible deterministic features are masked by noise.

## ACKNOWLEDGMENTS

We thank K. Gulden and M. Moser of the CSEM, Zürich (formerly the Paul Scherrer Institute) for providing us with the lasers. This work was partially supported by the European Strategic Program for Research and Development in Information Technology (ACQUIRE 20029), by CNR Contract Nos. 96.00267.CT02, 97.00073.CT02, and 98.00444.PF48 (MADESS), by the EEC Contract No. ERBFMRXCT960010, and by the PAIS project ‘‘Quantum noise reduction in semiconductor optical systems’’ of the INFN (Istituto Nazionale per la Fisica della Materia).

- 
- [1] C.J. Chang-Hasnain, M. Orenstein, A.C. Von Lehmen, L.T. Florez, J.P. Harbison, and N.G. Stoffel, *Appl. Phys. Lett.* **57**, 218 (1990).  
 [2] K. Tai, Y. Lai, K.F. Huang, T.C. Huang, T.D. Lee, and C.C.

- Wu, *Appl. Phys. Lett.* **63**, 2624 (1993).  
 [3] D.L. Huffaker, D.G. Deppe, and T.J. Rogers, *Appl. Phys. Lett.* **65**, 1611 (1994).  
 [4] F.B. de Colstoun, G. Khitrova, V.A. Fedorov, T.R. Nelson, C.

- Lowry, T.M. Brennan, B.G. Hammons, and P.D. Maker, *Chaos Solitons Fractals* **4**, 1575 (1994).
- [5] A.K. Jansen van Doorn, M.P. van Exter, and J.P. Woerdman, *Electron. Lett.* **30**, 1941 (1994).
- [6] C.J. Chang-Hasnain, J.P. Harbison, G. Hasnain, A.C. Von Lehmen, L.T. Florez, and N.G. Stoffel, *IEEE J. Quantum Electron.* **27**, 1402 (1991).
- [7] K.D. Choquette, D.A. Richie, and R.E. Leibenguth, *Appl. Phys. Lett.* **64**, 2062 (1994).
- [8] H. Li, T.L. Lucas, J. McInerney, and R.A. Morgan, *Chaos, Solitons and Fractals* **4**, 1619 (1994).
- [9] J.E. Epler, S. Gehrsitz, K.H. Gulden, M. Moser, H.C. Sigg, and H.W. Lehmann, *Appl. Phys. Lett.* **69**, 722 (1996).
- [10] E. Goobar, J.W. Scott, B. Thibeault, G. Robinson, Y. Akulova, and L.A. Coldren, *Appl. Phys. Lett.* **67**, 3697 (1995).
- [11] D.V. Kuksenkov, H. Temkin, and S. Swirhun, *Appl. Phys. Lett.* **67**, 2141 (1995).
- [12] D.C. Kilper, P.A. Roos, J.L. Carlsten, and K.L. Lear, *Phys. Rev. A* **55**, R3323 (1997).
- [13] J.-L. Vey and W. Elsässer, *Opt. Lett.* **23**, 721 (1998).
- [14] G. Giacomelli, F. Marin, M. Gabrysch, K.H. Gulden, and M. Moser, *Opt. Commun.* **146**, 136 (1998).
- [15] G. Giacomelli and F. Marin, *Quantum Semiclass. Opt.* **10**, 1 (1998).
- [16] M. Travagnin, M.P. van Exter, and J.P. Woerdman, *Phys. Rev. A* **56**, 1497 (1997).
- [17] M. San Miguel, Q. Feng, and J.V. Moloney, *Phys. Rev. A* **52**, 1728 (1995).
- [18] M.B. Willemsen, M.U.F. Khalid, M.P. van Exter, and J.P. Woerdman, *Phys. Rev. Lett.* **82**, 4815 (1999).
- [19] M.P. van Exter, M.B. Willemsen, and J.P. Woerdman, *Phys. Rev. A* **58**, 4191 (1998).
- [20] J. Martin-Regalado, S. Balle, and M. San Miguel, *Opt. Lett.* **22**, 460 (1997).
- [21] J. Martin-Regalado, S. Balle, M. San Miguel, A. Valle, and L. Pesquera, *Quantum Semiclass. Opt.* **9**, 713 (1997).
- [22] F. Marin and G. Giacomelli, *J. Opt. B: Quantum Semiclass. Opt.* **1**, 128 (1999).
- [23] K.H. Gulden, M. Moser, S. Lüscher, and H.P. Schweizer, *Electron. Lett.* **31**, 2176 (1995).
- [24] P. Hänggi, P. Talkner, and M. Borkovec, *Rev. Mod. Phys.* **62**, 251 (1990).
- [25] M. San Miguel, in *Semiconductor Quantum Optoelectronics*, edited by A. Miller, M. Ebrahimzadeh, and D.M. Finlayson (IOP, Bristol, 1999), pp. 339–366.
- [26] J. Martin-Regalado, M. San Miguel, N.B. Abraham, and F. Prati, *Opt. Lett.* **53**, 122 (1996).
- [27] J. Martin-Regalado, F. Prati, M. San Miguel, and N.B. Abraham, *IEEE J. Quantum Electron.* **33**, 765 (1997).
- [28] F. Prati, A. Tesei, L.A. Lugiato, and R.J. Horowicz, *Chaos Solitons Fractals* **4**, 1637 (1994).
- [29] F. Prati, M. Travagnin, and L.A. Lugiato, *Phys. Rev. A* **55**, 690 (1997).
- [30] R.F.M. Hendriks, M.P. van Exter, J.P. Woerdman, K.H. Gulden, and M. Moser, *IEEE J. Quantum Electron.* **34**, 1455 (1998).
- [31] P. Colet, M. San Miguel, M. Brambilla, and L.A. Lugiato, *Phys. Rev. A* **43**, 3862 (1991).
- [32] P. Grassberger and I. Procaccia, *Phys. Rev. Lett.* **50**, 346 (1983).